

# Bacterial Swimming Motility Enhances Cell Deposition and Surface Coverage

ALEXIS J. DE KERCHOVE AND  
MENACHEM ELIMELECH\*

Department of Chemical Engineering, Environmental  
Engineering Program, Yale University,  
P.O. Box 208286, New Haven, Connecticut 06520-8286

Received December 4, 2007. Revised manuscript received  
March 21, 2008. Accepted March 24, 2008.

The influence of bacterial motility on cell transport and deposition was investigated in a well-characterized radial stagnation point flow (RSPF) chamber. Deposition experiments were conducted with nonmotile (PAO1  $\Delta fliC \Delta pilA$ ) and motile (PAO1  $\Delta pilA$ ) strains of *Pseudomonas aeruginosa*, and oppositely (positively) charged modified quartz surfaces. Deposition dynamics of the two bacterial strains were determined over a wide range of solution ionic strengths and at two flow velocities. The observed deposition dynamics were modeled using a modified expression of the random sequential adsorption (RSA) blocking function accounting for the impacts of hydrodynamic and electrostatic interactions on cell deposition. Results for the nonmotile bacteria indicated that the changes in blocking rate and surface coverage with ionic strength and flow rate were similar to those expected for nonbiological, “soft” particles, for which the coupling of hydrodynamic interactions and electrostatic repulsion governs the deposition dynamics. In contrast, deposition dynamics of the motile bacterial cells reduced blocking rates and enhanced maximum coverages, approaching the jamming limit predicted for “hard” ellipsoids of 0.583. We hypothesized that cell motility allows the upstream swimming of bacteria and subsequent cell deposition on regions which are otherwise inaccessible to nonmotile cell deposition due to the “shadow effect”.

## Introduction

Transport and deposition of bacteria in aquatic systems are of fundamental importance in a variety of fields, including wastewater treatment (1), groundwater bioremediation (2), and biomedical applications (3). Such systems are often continuously exposed to microorganisms, which results in cell deposition at the solid–water interface and biofouling (4). Rigorous analysis of the time-dependence of bacterial deposition rates, known as deposition dynamics, can be useful to gain a better understanding of the impact of the continuous exposure of engineered and natural surfaces to bacterial fluxes.

Previous studies on the deposition dynamics of nonmotile bacteria in porous media under flow conditions have indicated similarities between the deposition responses of bacterial cells and nonbiological, “soft” colloidal particles (5, 6). The initial stage of particle deposition is characterized

by a constant deposition rate due to low particle coverage on the collector surface. However, as deposited particles accumulate at the collector surface, the rate of particle deposition starts to decline (7). The surface exclusion to further deposition, or surface blocking (7, 8), has been described as a function of tangential hydrodynamic forces and electrostatic repulsion between approaching and deposited particles. The coupling of these forces results in a “shadow” region on the collector surface down-gradient of deposited particles, where the probability of subsequent deposition is significantly reduced. Studies on deposition dynamics have demonstrated that the size of the shadow region is defined by the physicochemical conditions of the system, such as the ionic strength and flow conditions (7). For example, surface blocking was significantly reduced with increasing ionic strength (i.e., decreasing electrostatic repulsion between particles) and decreasing flow velocity (i.e., decreasing tangential shear forces between the surface and the particle) (7).

The dynamic blocking function for “hard” spheres depositing on an oppositely charged surface in a stagnant system was initially modeled by Schaaf and Talbot (9), who considered surface blocking in terms of a random sequential adoption (RSA) mechanism. However, in order to account for the impacts of colloidal interactions as well as system hydrodynamics, a modified expression of the RSA blocking function was developed as a virial expansion with surface coverage (10). In this expression, the virial coefficients were interpreted as a function of three interactions which contribute to surface blocking: hard sphere interactions, electrostatic repulsion, and hydrodynamic interactions (11). Similarly to the original RSA blocking function for hard spheres, the modified RSA blocking function assumes (9, 10) (i) particle–particle contact is prohibited at the collector surface (i.e., there is no overlapping of deposited particles to form a multilayer), (ii) particle deposition is irreversible, and (iii) no surface diffusion. The modified blocking function has been previously applied to describe the deposition of latex particles (11); however, this model has never been applied to predict the deposition dynamics of bacteria.

The dynamic properties of the bacterial surface in response to environmental stresses allow microorganisms to survive even in the most inhospitable aquatic systems (12). Among the numerous appendages anchored to the surface of bacteria, flagella are possibly the most important for their roles in the transport of planktonic cells and their transfer to solid substrates. Flagella are complex polymeric structures of glycoproteins that provide swimming ability to the cells (13). The active rotation of the flagellum filament induces the propulsion of the cell body which can reach speeds greater than 30  $\mu\text{m/s}$  (13). The presence of the flagella and the ability of the cell to swim are important factors which enhance the transport and initial deposition of cells onto alginate-conditioned substrates (14, 15). However, the effects of motility on the deposition dynamics of bacterial cells (i.e., the time-dependence of bacterial deposition rate) have not been reported in the literature.

In this paper, we studied the deposition dynamics of motile and nonmotile bacteria to determine the impact of swimming mobility on the dynamic blocking function and maximum attainable surface coverage. Experiments were conducted using two mutant strains of *Pseudomonas aeruginosa*, characterized by their ability to swim. Bacterial deposition dynamics were investigated under nonrepulsive conditions (favorable to deposition) as a function of ionic strength and flow velocity in a radial stagnation point flow

\* Corresponding author phone: (203)432-2789; fax: (203)432-2881; e-mail: menachem.elimelech@yale.edu.

(RSPF) chamber. We demonstrated reductions in surface blocking and increases in maximal surface coverage for the motile bacteria, which are attributed to the swimming motility of the bacteria. The dynamics of deposition of the motile bacteria showed a strong dependence on the physicochemical conditions of the system.

## Materials and Methods

**Model Bacterial Strains and Substrates.** The nonmotile, PAO1  $\Delta fliC \Delta pilA$ , and motile, PAO1  $\Delta pilA$ , strains of *Pseudomonas aeruginosa* were used as model bacteria. Twitching and swimming disabilities of the mutant strains were previously verified (16). Bacterial cells were shown to remain viable and to have a constant size under a range of ionic strengths (1–300 mM of KCl). The major and minor axes of both bacterial strains were determined to be  $2.30 \pm 0.48 \mu\text{m}$  and  $0.93 \pm 0.05 \mu\text{m}$ , which is equivalent to a volumetric spherical diameter of  $1.25 \mu\text{m}$  (16). The physicochemical properties of the surface of both PAO1  $\Delta fliC \Delta pilA$  and PAO1  $\Delta pilA$  have been extensively investigated in our recent publication (16). Similar electrophoretic mobilities have been observed for both strains over a range of ionic strengths (1–100 mM KCl) at ambient pH (pH 5.5–5.7); the surface charge density for both strains was  $430 \pm 40 \mu\text{C}/\text{cm}^2$  (16).

Liquid cultures of PAO1 strains were incubated in LB at  $37^\circ\text{C}$  and harvested at midexponential growth phase. The bacterial suspension was centrifuged (Sorvall RC 26 Plus) for 15 min at 1000g. The cell pellet was washed once with 100 mM KCl solution, recentrifuged under the same conditions, and resuspended in KCl (100 mM). The cell stock solution was diluted in electrolyte solutions of interest (1, 10, and 100 mM KCl). Ultrapure quartz coverslips measuring 25 mm in diameter and 0.1 mm thick (Electron Microscopy Sciences, PA) were used as the solid substrate in the deposition experiments. Coverslips were cleaned in a three-step process: (i) 2% Hellmanex II bath (overnight,  $75^\circ\text{C}$ ) (Hellma GmbH & CoKG, Germany), (ii) Nochromix bath (overnight,  $25^\circ\text{C}$ ) (Godax Laboratories, Inc., MD), and (iii) baking (1–3 h,  $560^\circ\text{C}$ ). Coverslips were thoroughly rinsed with DI water after steps (i) and (ii). Favorable (nonrepulsive) deposition conditions between the particles and the substrate were obtained by chemical modification of the coverslip surface. Charge reversal was induced by adsorption of a layer of poly-L-lysine (PLL) at the quartz surface. Poly-L-lysine hydrobromide (Sigma, MO) with an average molecular weight of 110 kDa was used. The quartz coverslips were submerged in 0.1 g/L PLL/HEPES solution (pH 5.6,  $0.22 \mu\text{m}$ -filtered) overnight at  $4^\circ\text{C}$ , and rinsed four times with  $0.22 \mu\text{m}$ -filtered DI water. The quartz coverslips were vacuum-dried for 3 h at  $37^\circ\text{C}$ . Charge reversal has been previously verified by electrophoretic mobility measurements of PLL-coated silica particle at ambient pH (pH 5.5–5.7) following a similar procedure (16).

**Deposition Kinetics in a Radial Stagnation Point Flow System.** Bacterial deposition onto a PLL-coated quartz substrate was investigated using a radial stagnation point flow system with contrast phase microscopy (Axiovert 200m, Zeiss). Deposition was recorded in a rectangular viewing area of  $220 \mu\text{m} \times 165 \mu\text{m}$  (captured in a  $140 \mu\text{m}$ -radius circle) with a DP70 digital camera (Olympus). Details on the hydrodynamic properties of the flow chamber can be found elsewhere (17). The injection capillary radius of the RSPF system was 1 mm; the distance between the capillary outlet and the collector surface was 2 mm. A constant flow rate of 4.93 mL/min (average capillary velocity = 2.65 cm/s) or 1.00 mL/min (average capillary velocity = 0.53 cm/s) was fixed by syringe pumps (KD Scientific Inc., PA) during the deposition experiments. For these velocities, the corresponding Reynolds number was 28.4 or 5.7, respectively, and the cell Peclet

number was 0.22 or 0.01, respectively (18). All experiments were conducted under the same hydrodynamic conditions, at ambient pH (5.5–5.7), and at  $25^\circ\text{C}$  ( $\pm 1^\circ\text{C}$ ).

Bacterial deposition was studied as a function of ionic strength (KCl) using reagent grade salt (Fisher Scientific). Deposition at 2.65 cm/s (average flow velocity) was measured at 15 s intervals for 30 min and deposition at 0.53 cm/s was measured at 20 s intervals for 3 h. For each culture, the cell concentration was determined in a Buerker-Tuerker cytometer chamber (Marienfeld Laboratory Glassware, Germany). For each bacterial deposition experiment, the bacterial transfer rate coefficient,  $k_{\text{RSPF}}$ , was calculated as the ratio between the bacterial deposition flux and the initial bacterial bulk concentration (19). The bacterial deposition flux is the observed deposition rate of bacteria normalized by the camera viewing area. All deposition rate coefficients are averages taken from two to three experiments conducted using different cell cultures. Matlab Particle Tracking Code (20) (MathWorks, Inc.) was used to count deposited cells. These values were confirmed by manual counting using the image processing program, Image J (NIH), and the interactive plugin, Point Picker (9).

**Analysis of Deposition Dynamics.** At high surface coverage, the deposition dynamics of bacterial cells on a surface can be described by the following rate equation (21, 22):

$$\frac{\partial \theta}{\partial t} = \alpha \pi r_{p1} r_{p2} n_0 k_s B(\theta) \quad (1)$$

where  $\theta$  is the fractional coverage of the surface by depositing bacterial cells,  $\alpha$  is the particle attachment efficiency,  $r_{p1}$  and  $r_{p2}$  are the half-major and minor axes of an ellipsoid particle,  $n_0$  is the particle number concentration,  $k_s$  is the surface-limited cell deposition rate, and  $B(\theta)$  is the dynamic blocking function. To facilitate the solution of this differential equation, we assumed that  $k_s \approx k_{\text{RSPF}}$ , as was done in numerous past studies (7, 11, 23), with  $k_{\text{RSPF}}$  being the transport-limited cell deposition rate in the RSPF system. The fractional coverage can be determined from the number of deposited cells,  $n$ , included in the microscope's viewing area of  $220 \mu\text{m} \times 165 \mu\text{m}$ . Individual coverage per cell was based on the average calculated elliptic (side-on) projected surface area of the cells. The attachment efficiency represents the fraction of cell contacts with the substrate that result in attachment; for our case of cell deposition on PLL-coated substrate,  $\alpha = 1$ .

In the RSA model for hard spherical particles, the dynamic blocking function,  $B(\theta)$ , is given by (10)

$$B(\theta) = 1 - 4\theta + \frac{6\sqrt{3}}{\pi}\theta^2 + \left(\frac{40}{\pi\sqrt{3}} - \frac{176}{3\pi^2}\right)\theta^3 + \dots \quad (2)$$

However, this model is not valid for our study where both hydrodynamic and electrostatic interactions play important roles in bacterial deposition dynamics. Through application of the virial expansion theory, the dynamic blocking function,  $B(\theta)$ , can be represented as a series expansion in  $\theta$  as indicated by (24)

$$B(\theta) = 1 + a_1\theta + a_2\theta^2 + a_3\theta^3 + \dots \quad (3)$$

This function is valid for surface coverage of up to about 0.8 times the maximum attainable surface coverage, or jamming limit,  $\theta_{\text{max}}$  (= 0.583 for hard ellipsoids (10) with an aspect ratio of 2:1) (11).

The virial coefficients ( $a_1$ ,  $a_2$ , and  $a_3$ ) were estimated using eqs 1 and 3, following the numerical procedure described by Ko et al. (11, 23). The boundary conditions for the governing equation (eq 1) are  $\theta(0) = 0$  and  $\theta(t \rightarrow \infty) = \theta_{\text{max}}$ . Previously, similar approaches have been shown to provide good correlation with experimental data (23, 25). Since mass transfer was constant across the stagnation point flow area

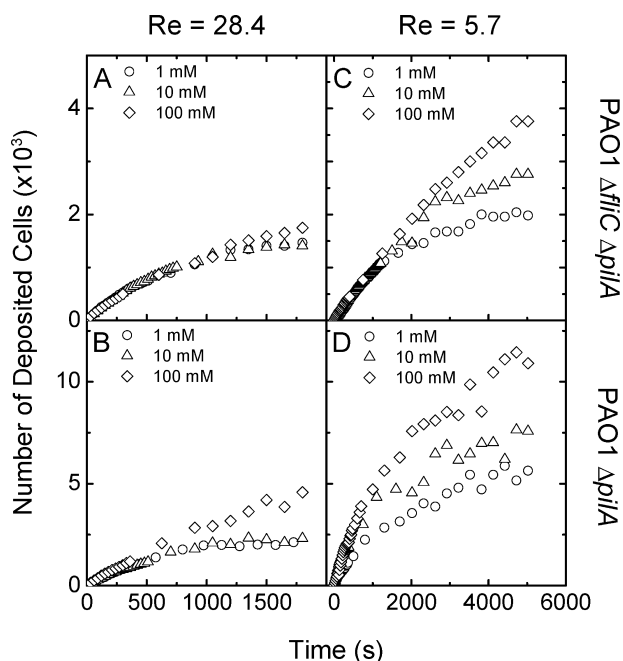


**FIGURE 1.** Bacterial deposition of PAO1  $\Delta fliC \Delta pilA$  and PAO1  $\Delta pilA$  under favorable conditions as a function of ionic strength (KCl) and Reynolds number (flow velocity). The reported number of deposited cells in the microscope's viewing area ( $220 \mu\text{m} \times 165 \mu\text{m}$ ). The capillary flow rate in the RSPF system was either 4.93 mL/min (average velocity of 2.65 cm/s) for Panels A and B or 1.00 mL/min (average velocity of 0.53 cm/s) for Panels C and D. The corresponding capillary Reynolds numbers were 28.4 and 5.7, respectively, and the cell Peclet numbers were 0.22 and 0.01, respectively. Other experimental conditions employed were ambient pH (pH 5.5–5.7) and a temperature of  $25 \text{ }^\circ\text{C}$  ( $\pm 1 \text{ }^\circ\text{C}$ ).

in our experiments, time was represented as a dimensionless variable in our analyses (26):

$$\tau = \pi r_{p1} r_{p2} k_{\text{RSPF}} n_0 t \quad (4)$$

The maximum attainable surface coverage,  $\theta_{\text{max}}$ , for the various physicochemical conditions was calculated using the estimated values of the three virial coefficients with  $B(\theta) = 0$  (i.e., when  $\theta = \theta_{\text{max}}$ , eq 3).

## Results and Discussion

**Cell Deposition Dynamics.** Deposition kinetics of motile PAO1  $\Delta pilA$  and nonmotile PAO1  $\Delta fliC \Delta pilA$  cells were determined in the RSPF system as a function of ionic strength and flow velocity (Figure 1) under favorable deposition conditions (i.e., electrostatic attraction between cells and PLL-coated quartz). Under all experimental conditions, the number of deposited cells increased nonlinearly with time. Increasing surface coverage by adhering cells reduces the availability of the surface to further bacterial deposition, thereby creating a dynamic blocking effect.

Before blocking becomes significant, the initial slope of the bacterial deposition can be used to determine the initial deposition rate coefficient,  $k_{\text{RSPF}}$ , of the cells onto the substrate. Initial bacterial cell transfer rates were calculated (Figure 2) for both nonmotile and motile cells. Initial deposition rates of nonmotile bacteria (PAO1  $\Delta fliC \Delta pilA$ ) were not sensitive to changes in ionic strength; however, deposition rates significantly decreased with a reduction of flow velocity. These deposition responses were similar to those observed previously for nonbiological colloidal particles under transport limited conditions (9).

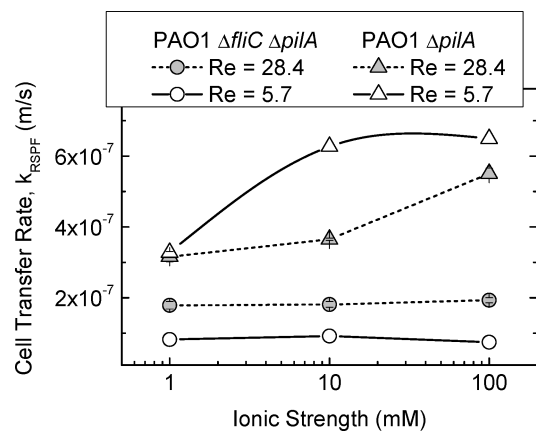


**FIGURE 2.** Deposition kinetics of PAO1  $\Delta fliC \Delta pilA$  and PAO1  $\Delta pilA$  under favorable conditions (i.e., electrostatic attraction between cells and PLL coated quartz) as a function of ionic strength (KCl) and Reynolds number. Deposition kinetics are expressed as a cell transfer rate,  $k_{\text{RSPF}}$ . The capillary flow rate in the RSPF system was either 4.93 mL/min (average velocity of 2.65 cm/s) (in gray dashed lines) or 1.00 mL/min (average velocity of 0.53 cm/s) (in black solid lines). The corresponding capillary Reynolds numbers were 28.4 and 5.7, respectively, and the cell Peclet numbers were 0.22 and 0.01, respectively. Other experimental conditions employed were ambient pH (pH 5.5–5.7) and a temperature of  $25 \text{ }^\circ\text{C}$  ( $\pm 1 \text{ }^\circ\text{C}$ ). Error bars indicate one standard deviation.

In contrast, the initial deposition rate of motile bacteria (PAO1  $\Delta pilA$ ) significantly increased with both increasing ionic strength and decreasing flow velocity (Figure 2). The differences in deposition responses to changes in ionic strength can be attributed to the impact of the electrolyte concentration on bacterial motility. In addition, opposite responses in initial deposition rates for motile and nonmotile bacteria were observed upon decreasing flow velocity. Since the two bacterial strains were shown to have an equivalent cell size and shape, no differences in diffusion rates were expected between the two strains. Therefore, this suggests that the increase in deposition rate of motile cells with decreasing flow velocity is a result of increased bacterial motility (i.e., enhanced swimming) due to a reduction in hydrodynamic interactions.

Over long deposition times, significant reductions in the deposition kinetic slopes for both bacterial strains were observed as a result of enhanced blocking of the collector surface (Figure 1). The dynamic blocking effect was observed to be more pronounced for nonmotile bacteria compared to motile bacteria. However, both bacterial strains indicated an increase in blocking effect for decreasing ionic strengths and increasing flow velocities. Due to experimental constraints limiting the time-scale of the deposition experiments, we were not able to extract exact approximations of maximum surface coverage for the studied systems directly from our raw deposition data.

### Virial Coefficients of the Dynamic Blocking Function.

Inverse analysis was performed by fitting the numerical solution of eq 1 to the bacterial deposition data (Figure 1) while simultaneously optimizing for the three virial coefficients  $a_1$ ,  $a_2$ , and  $a_3$ . Equation 3 was used as the dynamic blocking function in the fittings. Initial deposition rate coefficients,  $k_{\text{RSPF}}$ , for each bacterial strain are provided in Figure 2. The accuracy of the analysis was verified by comparing the observed deposition dynamics to their fitted solution for each physicochemical condition used in our system (Figures 3 and 4). The fitted curves showed excellent visual agreement with the deposition curves of both nonmotile (PAO1  $\Delta fliC \Delta pilA$ ) and motile (PAO1  $\Delta pilA$ ) bacteria

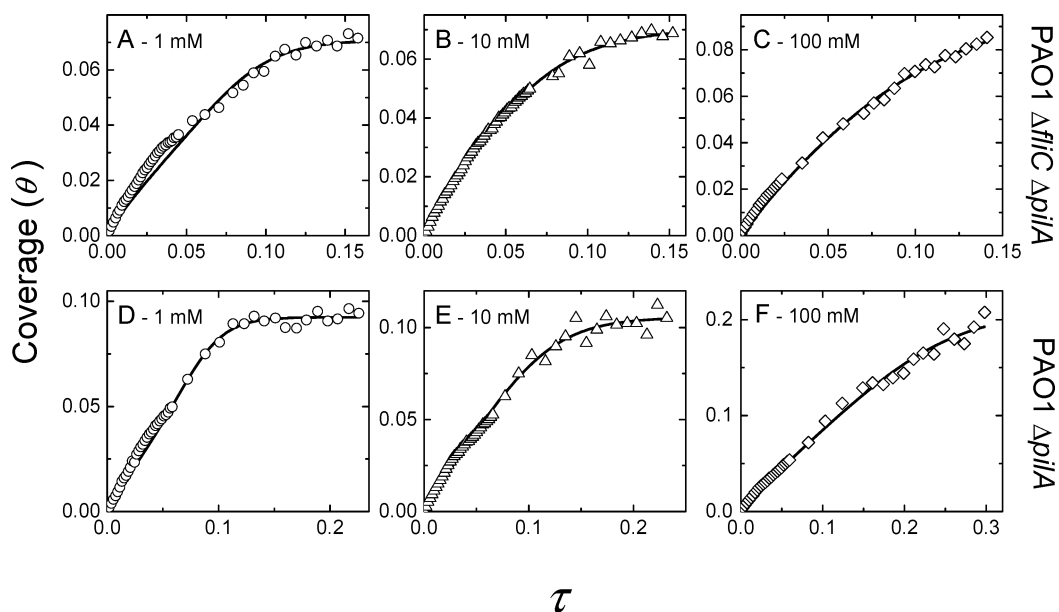


**FIGURE 3.** Comparison of experimental (symbols) and theoretical (solid lines) values of fractional coverage for PAO1  $\Delta$ *fliC*  $\Delta$ *pilA* (Panels A, B, and C) and PAO1  $\Delta$ *pilA* (D, E, and F) at 1, 10, and 100 mM KCl and an average flow velocity of 2.65 cm/s ( $Re = 28.4$ ). The theoretical model was based on the modified RSA blocking functions (24). Experimental values of the fractional coverage were calculated from deposition data (Figure 1) considering the elliptic projected surface area for the cells and a microscope's viewing area of  $220 \times 165 \mu\text{m}$ .

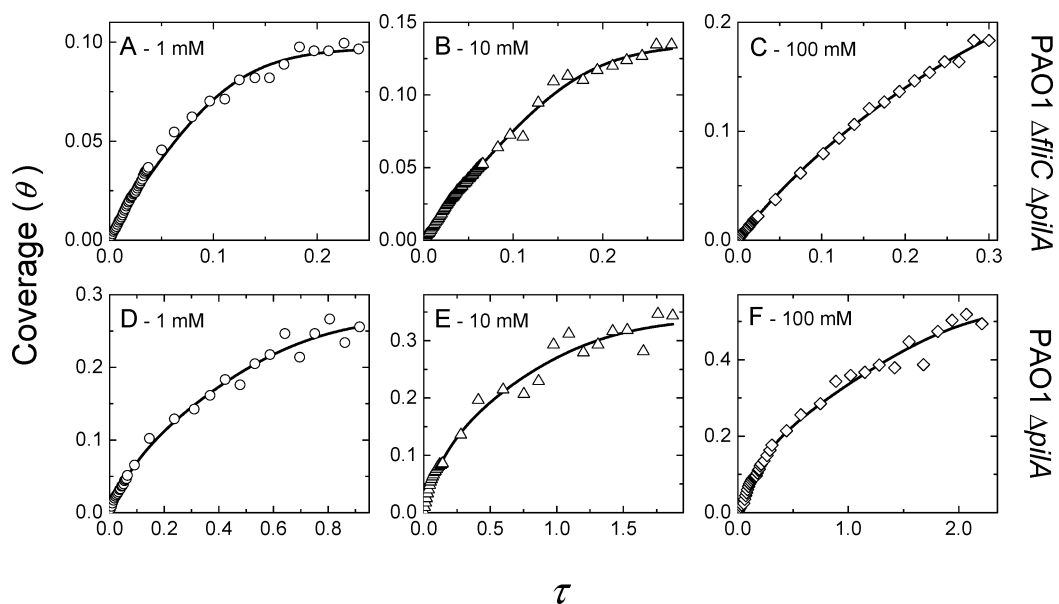


**FIGURE 4.** Comparison of experimental (symbols) and theoretical (solid lines) values of fractional coverage for PAO1  $\Delta$ *fliC*  $\Delta$ *pilA* (Panels A, B, and C) and PAO1  $\Delta$ *pilA* (Panels D, E, and F) at 1, 10, and 100 mM KCl and an average flow velocity of 0.53 cm/s ( $Re = 5.7$ ). The theoretical model was based on the modified RSA blocking functions (24). Experimental values of the fractional coverage were calculated from deposition data (Figure 1) considering an elliptic area for the cells and a microscope's viewing area of  $220 \times 165 \mu\text{m}$ .

over the entire range of ionic strengths at the two different flow velocities, 2.65 cm/s ( $Re = 28.4$ , Figure 3) and 0.53 cm/s ( $Re = 5.7$ , Figure 4).

A direct dependence on both the electrostatic and hydrodynamic conditions of the system was observed for all three virial coefficients,  $a_1$ ,  $a_2$ , and  $a_3$  (Figure 5) for the two bacterial strains. In all cases, virial coefficients were observed to decrease with increasing ionic strength; these decreases were almost linear on a logarithmic scale. In addition, virial coefficients under low flow velocities ( $Re = 5.7$ ) were significantly smaller than those obtained under high flow

velocities ( $Re = 28.4$ ). The virial coefficients  $a_2$  and  $a_3$  were especially sensitive to these velocity changes.

The system response to increases in electrolyte concentrations and decreases in flow velocities is a result of decreases in electrostatic interactions between the approaching and deposited cells and decreases in tangential hydrodynamic forces that reduce surface blocking, respectively. Therefore, high ionic strengths and low flow velocities will simulate a system which begins to approach the RSA model conditions for hard particles. At high ionic strength (i.e., 100 mM) under both flow velocities, the virial coefficient  $a_1$  converged toward

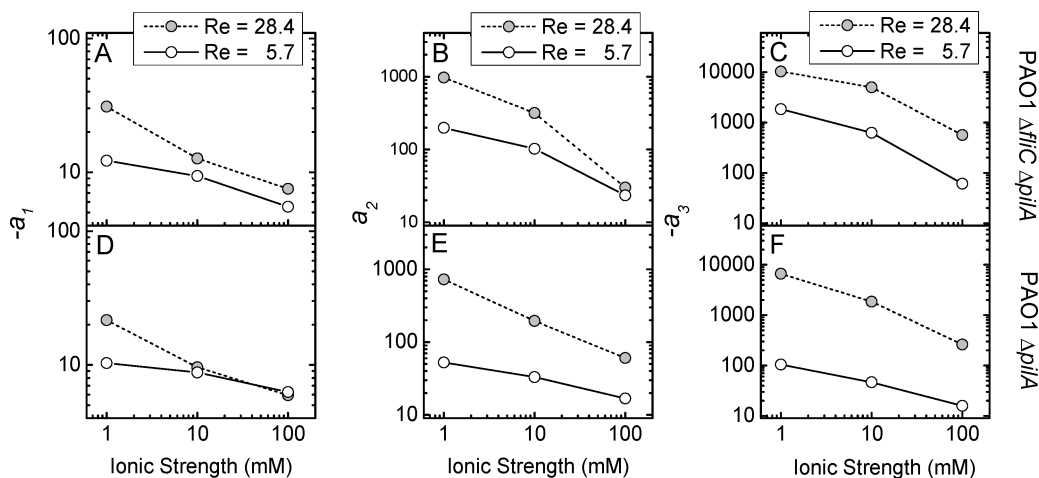


**FIGURE 5.** Variation of the three virial coefficients of the dynamic blocking function as a function of ionic strength and the average flow velocity (Reynolds number) for nonmotile PAO1  $\Delta fliC \Delta pilA$  (Panels A, B, and C) and motile PAO1  $\Delta pilA$  (Panels D, E, and F). Lines do not represent modeling results.

the known limiting value for hard spheres calculated from the RSA blocking function (eq 2,  $a_1 = -4$ ) (9). However, the virial coefficients  $a_2$  and  $a_3$  did not approach their respective limiting values for hard spheres (i.e.,  $a_2 = 3.3$  and  $a_3 = 1.4$ ) (7), especially under high flow velocity. Even at low flow velocities,  $a_2$  and  $a_3$  maintained absolute values greater than those predicted by the hard particle RSA model, which suggests that both hydrodynamic and electrostatic interactions between the cells remain important.

To determine the impact of cell motility on bacterial deposition and surface blocking, the three virial coefficients of motile and nonmotile bacteria cells were compared (Supporting Information Figure S1 and Figure 5). Virial coefficients of both bacterial strains at high flow velocity (Re = 28.4) were equivalent in magnitude, which suggests that under conditions where hydrodynamic interactions predominate, motility has no effect on the surface blocking of flagellated cells. However, under low flow velocity (Re = 5.7), the virial coefficients of motile cells were significantly smaller in magnitude than those of nonmotile cells; this effect was especially pronounced for  $a_2$  and  $a_3$ . This discrepancy between the two strains at low flow velocities suggests that motile cells have lower surface blocking rates than nonmotile bacteria. Therefore, motile bacteria have access to a larger available surface area for deposition.

**The Maximum Fractional Surface Coverage.** Maximum attainable surface coverage ( $\theta_{max}$ ) was calculated from eq 3 using the three estimated virial coefficients (Figure 6) by setting  $B(\theta) = 0$  when  $\theta = \theta_{max}$ . Maximum attainable surface coverages of motile PAO1  $\Delta pilA$  and nonmotile PAO1  $\Delta fliC \Delta pilA$  cells were determined as a function of ionic strength and flow velocity (Figure 8). For both bacterial strains, the maximum surface coverage increased with increasing ionic strength, as well as with decreasing flow velocity.

For nonmotile bacteria (Figure 6A), maximum surface coverage predicted under high ionic strength (100 mM) and low flow velocity (Re = 5.7) was more than two times the predicted coverage at low ionic strength (1 mM) and high flow velocity (Re = 28.4). This deposition trend is similar to that observed for noncolloidal soft particles subjected to the shadow effect (24). Predicted maximum surface coverages of nonmotile cells were always significantly smaller than the jamming limit ( $\theta_{\infty} = 0.583$ ) predicted for hard ellipsoids (with an aspect ratio of 2:1). This suggests that electrostatic and hydrodynamic interactions between the nonmotile cells remain important, and that significant blocking persists at the substrate surface.

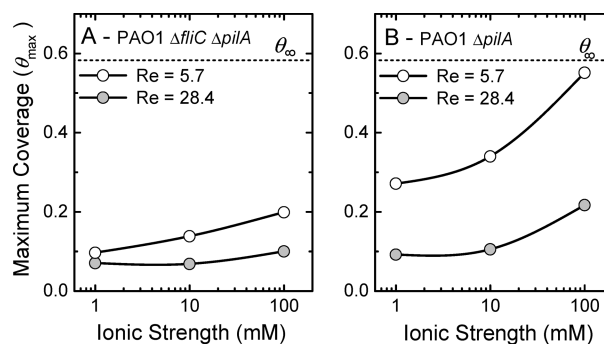


**FIGURE 6.** Theoretical variation of the maximum attainable fractional surface coverage as a function of ionic strength and average flow velocity (Reynolds number). Maximum coverage for PAO1  $\Delta fliC \Delta pilA$  (Panel A) and PAO1  $\Delta pilA$  (Panel B) was estimated by theoretical modeling of deposition kinetics using the RSA blocking function (eq 3). The dashed line labeled  $\theta_{\infty}$  (= 0.583) corresponds to the jamming limit for hard ellipsoids (of aspect ratio 2:1).

For similar physicochemical conditions, the maximum coverage of motile cells (Figure 6B) was always significantly larger than that of nonmotile cells (Figure 6A), indicating that swimming motility does affect maximum coverage predictions. The observed differences in maximum coverage were most pronounced at high ionic strength and low flow velocity. These physicochemical conditions are expected to enhance cell motility while minimizing the “shadow effect” and the electrostatic repulsion between cells. At high ionic strength (100 mM) and low flow velocity (Re = 5.7), predicted maximum coverage of motile cells approached the maximum jamming limit of hard ellipsoids ( $\theta_{\infty} = 0.583$ ). However, because of the potential interdependence between these physicochemical effects, individual impacts on the enhancements of the surface coverage by motile cells cannot be distinguished.

#### Influence of Bacterial Motility on Deposition Dynamics.

The impact of motility on surface coverage was determined using three attributes derived either experimentally or theoretically from the bacterial deposition experiments. These attributes were (i) the initial deposition rate, (ii) the magnitude of the three virial coefficients, and (iii) the predicted maximum surface coverage.

Initial deposition rate, in the absence of surface blocking, indicated that there is a strong dependence of cell motility on the solution ionic strength and flow velocity

(Figure 2). Significant enhancement in the deposition of cells onto the substrate was observed for high ionic strengths and low flow velocities. Our estimates of the virial coefficient as well as the prediction of maximal surface coverage suggested that cell motility significantly reduced the surface blocking rate (Figure 1), thereby favoring large surface coverage. The swimming propulsion of motile cells can be considered as a competitive kinetic force between electrostatic and hydrodynamic forces on the approach of the cell to the vicinity of other deposited cells.

The impact of ionic strength on cell motility can be explained by the environmental requirements of the biological functions of the flagellum. Swimming motility was enhanced at 100 mM KCl (Figure 2). This ionic strength approaches the ionic strength of physiological saline conditions (0.9% NaCl or ionic strength of 154 mM) that are optimal to induce flagella rotation (27). The flagella's motor is based on the coupling of electrochemical potentials across the cell membrane and electrostatic interactions between fixed charges on the flagella and the proton flux across the membrane (28). This complex mechanism relies on electrostatic interactions and, therefore, requires a strong electrolyte balance in its surrounding environment (29).

An increase in deposition as a result of decreasing flow velocity demonstrates the importance of convective flow on the degree of freedom of the swimming cell. A reduction in the Peclet number from 0.22 to 0.01 as flow velocity is reduced has been shown to allow bacterial cells to adopt a swimming behavior which approaches the fully random motility of cells in stagnant solutions (30). Random swimming in three dimensions increases the probability of the cell to reach the vicinity of the substrate, where physicochemical interactions can induce cell attachment (31). Our results suggest that bacterial motility controls the transport of the cell toward the substrate under reduced flow velocity conditions. Additional biological features of motile cells that influence their transport and can be affected by changes in physicochemical conditions are (i) changes in swimming direction when colliding with an obstacle (32), (ii) chemotaxis (33), and (iii) quorum sensing (34). Under optimal conditions, these features favor the direct displacement of the cells toward the substrate and increase the probability of finding available deposition sites at the surface.

Our observations of enhanced cell deposition and surface coverage under limited hydrodynamic conditions indirectly demonstrate the ability of our monoflagellated bacterial strain to swim upstream (i.e., against the radial flow in the RSPF). This interpretation is confirmed by the visual observation of upstream swimming by motile cells during deposition experiments under low flow velocity (video in Supporting Information). Hill et al. (34) recently demonstrated that multiflagellated bacteria actively swim against a flow field, which strongly supports our interpretations. *Escherichia coli* was demonstrated to swim preferentially upstream in a parallel plate flow chamber under a flow velocity of 1.62 cm/s (10) (i.e.,  $Re = 4.0$ ,  $Pe = 0.66$  assuming an equivalent spherical diameter of 1  $\mu\text{m}$  for *E. coli* cells). These conditions are similar to those employed in our experiments.

Therefore, our results suggest that upstream swimming of the cell is regulated by both the solution ionic strength and the flow velocity. We showed that the ionic strength strongly impacts flagellar motility and that the flow velocity defines the degree of freedom of cell motility. The ability of the cell to swim upstream and overcome hydrodynamic interactions provides these planktonic cells access to the "shadow" regions of the surface which are otherwise inac-

cessible to nonmotile cells (Supporting Information Figure S2). In this respect, reduction of the flow velocity will indirectly reduce the size of the shadow region during the deposition of motile bacteria. The size of the shadow region can be reduced until complete inhibition is obtained; at this point the approach distance between cells is strictly defined by the colloidal (electrostatic) interactions forces that persist between them.

## Acknowledgments

Funding was provided by the Water CAMPWS, a Science and Technology Center of Advanced Materials for the Purification of Water with Systems, under the National Foundation agreement, number CTS-0120978.

## Note Added after ASAP Publication

Due to a production error, the version of this paper that was published ASAP on May 7, 2008 contained errors throughout the text; the corrected version published ASAP May 17, 2008.

## Supporting Information Available

Comparison of the three virial coefficients of the motile and nonmotile bacteria (Figure S1); schematics of cell deposition enhancement by swimming motility (Figure S2). Also provided is a separate video file showing upstream swimming and subsequent deposition of flagellated *Pseudomonas aeruginosa* PAO1  $\Delta\text{pilA}$ .

## Literature Cited

- Miura, Y.; Watanabe, Y.; Okabe, S. Membrane biofouling in pilot-scale membrane bioreactors (MBRs) treating municipal wastewater: Impact of biofilm formation. *Environ. Sci. Technol.* **2007**, *41*, 632–638.
- Castro, F. D.; Tufenkji, N. Relevance of nontoxigenic strains as surrogates for *Escherichia coli* O157: H7 in groundwater contamination potential: Role of temperature and cell acclimation time. *Environ. Sci. Technol.* **2007**, *41*, 4332–4338.
- Tenke, P.; Kovacs, B.; Jackel, M.; Nagy, E. The role of Biofilm infection in urology. *World J. Urol.* **2006**, *24*, 13–20.
- O'Toole, G.; Kaplan, H. B.; Kolter, R. Biofilm formation as microbial development. *Annu. Rev. Microbiol.* **2000**, *54*, 49–79.
- Bolster, C. H.; Mills, A. L.; Hornberger, G. M.; Herman, J. S. Effect of surface coatings, grain size, and ionic strength on the maximum attainable coverage of bacteria on sand surfaces. *J. Contam. Hydrol.* **2001**, *50*, 287–305.
- Rijnaarts, H. H. M.; Norde, W.; Bouwer, E. J.; Lyklema, J.; Zehnder, A. J. B. Bacterial deposition in porous media related to the clean bed collision efficiency and to substratum blocking by attached cells. *Environ. Sci. Technol.* **1996**, *30*, 2869–2876.
- Johnson, P. R.; Elimelech, M. Dynamics of colloid deposition in porous-media—Blocking Based on Random Sequential Adsorption. *Langmuir* **1995**, *11*, 801–812.
- Ko, C. H.; Elimelech, M. The "shadow effect" in colloid transport and deposition dynamics in granular porous media: Measurements and mechanisms. *Environ. Sci. Technol.* **2000**, *34*, 3681–3689.
- Schaaf, P.; Talbot, J. Surface exclusion effects in adsorption processes. *J. Chem. Phys.* **1989**, *91*, 4401–4409.
- Warszynski, P. Coupling of hydrodynamic and electric interactions in adsorption of colloidal particles. *Adv. Colloid Interface Sci.* **2000**, *84*, 47–142.
- Ko, C. H.; Bhattacharjee, S.; Elimelech, M. Coupled influence of colloidal and hydrodynamic interactions on the RSA dynamic blocking function for particle deposition onto packed spherical collectors. *J. Colloid Interface Sci.* **2000**, *229*, 554–567.
- Klausen, M.; Heydorn, A.; Ragas, P.; Lambertsen, L.; Aaes-Jorgensen, A.; Molin, S.; Tolker-Nielsen, T. Biofilm formation by *Pseudomonas aeruginosa* wild type, flagella and type IV pili mutants. *Mol. Microbiol.* **2003**, *48*, 1511–1524.
- Doyle, T. B.; Hawkins, A. C.; McCarter, L. L. The complex flagellar torque generator of *Pseudomonas aeruginosa*. *J. Bacteriol.* **2004**, *186*, 6341–6350.
- Camesano, T. A.; Logan, B. E. Influence of fluid velocity and cell concentration on the transport of motile and nonmotile bacteria in porous media. *Environ. Sci. Technol.* **1998**, *32*, 1699–1708.
- Korber, D. R.; Lawrence, J. R.; Caldwell, D. E. Effect of motility on surface colonization and reproductive success of *Pseudomo-*

- nas fluorescens* in dual-dilution continuous-culture and batch culture systems. *Appl. Environ. Microbiol.* **1994**, *60*, 1421–1429.
- (16) de Kerchove, A. J.; Elimelech, M. Impact of alginate conditioning film on deposition kinetics of motile and nonmotile *Pseudomonas aeruginosa* strains. *Appl. Environ. Microbiol.* **2007**, *73*, 5227–5234.
- (17) de Kerchove, A. J.; Weroni, P.; Elimelech, M. Deposition of nonmotile *Pseudomonas aeruginosa* on “soft” polyelectrolyte layer in a radial stagnation point flow system: measurements and model predictions. *Langmuir* **2007**, *23*, 12301–12308.
- (18) Redman, J. A.; Walker, S. L.; Elimelech, M. Bacterial adhesion and transport in porous media: Role of the secondary energy minimum. *Environ. Sci. Technol.* **2004**, *38*, 1777–1785.
- (19) Matlab Particle Tracking. <http://www.seas.harvard.edu/projects/weitzlab/matlab/index.html>.
- (20) Point Picker. <http://bigwww.epfl.ch/thevenaz/pointpicker/>.
- (21) Talbot, J.; Schaaf, P.; Tarjus, G. Random sequential addition of hard-spheres. *Mol. Phys.* **1991**, *72*, 1397–1406.
- (22) Calonder, C.; Van Tassel, P. R. Kinetic regimes of protein adsorption. *Langmuir* **2001**, *17*, 4392–4395.
- (23) Adamczyk, Z.; Siwek, B.; Warszynski, P. Deposition of particles in the impinging-jet cell for the high coverage regime. *J. Colloid Interface Sci.* **2002**, *248*, 244–254.
- (24) Viot, P.; Tarjus, G.; Ricci, S. M.; Talbot, J. Random sequential adsorption of anisotropic particles 0.1. jamming limit and asymptotic-behavior. *J. Chem. Phys.* **1992**, *97*, 5212–5218.
- (25) Talbot, J.; Tarjus, G.; Schaaf, P. Unexpected asymptotic-behavior in random sequential adsorption of nonspherical particles. *Phys. Rev. A* **1989**, *40*, 4808–4811.
- (26) Elimelech, M. Effect of particle-size on the kinetics of particle deposition under attractive double-layer interactions. *J. Colloid Interface Sci.* **1994**, *164*, 190–199.
- (27) Berg, H. C. The rotary motor of bacterial flagella. *Annu. Rev. Biochem.* **2003**, *72*, 19–54.
- (28) Walz, D.; Caplan, S. R. An electrostatic model of the bacterial flagellar motor. *Bioelectrochem. Bioenerg.* **1998**, *47*, 19–24.
- (29) Berg, H. C. Motile behavior of bacteria. *Phys. Today* **2000**, *53*, 24–29.
- (30) Vigeant, M. A. S.; Ford, R. M.; Wagner, M.; Tamm, L. K. Reversible and irreversible adhesion of motile *Escherichia coli* cells analyzed by total internal reflection aqueous fluorescence microscopy. *Appl. Environ. Microbiol.* **2002**, *68*, 2794–2801.
- (31) Cisneros, L.; Dombrowski, C.; Goldstein, R. E.; Kessler, J. O. Reversal of bacterial locomotion at an obstacle. *Phys. Rev. E* **2006**, *73*.
- (32) Adler, J. Chemotaxis in Bacteria. *Annu. Rev. Biochem.* **1975**, *44*, 341–356.
- (33) Kusy, K.; Ford, R. T. Monte Carlo simulations derived from direct observations of individual bacteria inform macroscopic migration models at granular porous media interfaces. *Environ. Sci. Technol.* **2007**, *41*, 6403–6409.
- (34) Hill, J.; Kalkanci, O.; McMurry, J. L.; Koser, H. Hydrodynamic surface interactions enable *Escherichia coli* to seek efficient routes to swim upstream. *Phys. Rev. Lett.* **2007**, *98*.

ES703028U